

## Simultaneous synthesis and consolidation of a nanostructured $\text{Al}_2\text{TiO}_5$ compound by high-frequency induction heating

Hyun-Su Kang<sup>a</sup>, Hyun-Kuk Park<sup>a</sup>, Jung-Mann Doh<sup>b</sup>, Jin-Kook Yoon<sup>b</sup>, Seok-Jae Lee<sup>a</sup> and In-Jin Shon<sup>a,\*</sup>

<sup>a</sup>Division of Advanced Materials Engineering and the Research Center of Advanced Materials Development, Engineering College, Chonbuk National University, 561-756, Republic of Korea

<sup>b</sup>Advanced Functional Materials Research Center, Korea Institute of Science and Technology, PO Box 131, Cheongryang, Seoul 130-650, Republic of Korea

Nanopowders of  $\text{Al}_2\text{O}_3$  and  $\text{TiO}_2$  were made by high energy ball milling. The rapid synthesis and sintering of a nanostructured  $\text{Al}_2\text{TiO}_5$  compound were investigated by the high-frequency induction heated sintering process. The advantage of this process is that it allows very quick densification to near theoretical density and inhibition of grain growth. A highly dense nanostructured  $\text{Al}_2\text{TiO}_5$  compound was produced with simultaneous application of 80 MPa pressure and an induced current of total output power capacity (15 kW) within 3 minutes. The grain sizes of  $\text{Al}_2\text{TiO}_5$  sintered at 1250 °C and the hardnesses were investigated.

**Key words:** Sintering,  $\text{Al}_2\text{TiO}_5$ , Nanostructured material, Powder metallurgy.

### Introduction

Ceramics with low coefficients of thermal expansion represent an ever-increasing portion of the structural ceramics market because of their dimensional stability and high resistance to thermal shock.  $\text{Al}_2\text{TiO}_5$  is a good example. Owing to its near zero thermal expansion, low thermal conductivity and high melting point (1850 °C) [1, 2], it can be used as a thermal resistant material, such as in catalyst carriers for purification of the fume produced by cars, as containers and tubes for storing or conveying high temperature liquid steel and as a protective tube for thermocouples, etc. However, as in the case of many ceramic materials, the current concern about these materials focuses on their low fracture toughness below the ductile-brittle transition temperature. To improve their mechanical properties, the approach commonly utilized has been the addition of a second phase to form composites and to make nanostructured materials.

Nanocrystalline materials have received much attention as advanced engineering materials with improved physical and mechanical properties [3, 4]. As nanomaterials possess high strength, high hardness, excellent ductility and toughness, undoubtedly, more attention has been paid for their application [5, 6]. In recent days, nanocrystalline powders have been developed by the thermochemical and thermomechanical process named the spray conversion process (SCP), co-precipitation and high energy milling

[7~9]. However, the grain size in sintered materials becomes much larger than that in pre-sintered powders due to rapid grain growth during the conventional sintering process. Therefore, even though the initial particle size is less than 100 nm, the grain size increases rapidly up to 2  $\mu\text{m}$  or larger during the conventional sintering [10]. So, controlling grain growth during sintering is one of the keys to the commercial success of nanostructured materials. In this regard, the high-frequency induction heated sintering method (HFIHSM) which can make dense materials within 2 minutes has been shown to be effective in achieving this goal [11-13].

In this study, we investigated the synthesis and sintering of the  $\text{Al}_2\text{TiO}_5$  compound by the HFIHSM method. The goal of this research is to produce dense nanostructured  $\text{Al}_2\text{TiO}_5$  material. In addition, we also studied the microstructure and mechanical properties of the  $\text{Al}_2\text{TiO}_5$  compound.

### Experimental procedure

The  $\text{TiO}_2$  powder with a grain size of < 45  $\mu\text{m}$  and 99.8 % purity and  $\text{Al}_2\text{O}_3$  powder with a grain size of < 3  $\mu\text{m}$  and 99.99% purity used in this research were supplied by Alfa. The powders ( $\text{TiO}_2\text{-Al}_2\text{O}_3$ ) were first milled in a high-energy ball mill (Pulverisette-5 planetary mill) at 250 rpm for 4 h. Tungsten carbide balls (9 mm in diameter) were used in a sealed cylindrical stainless steel vial under an argon atmosphere. The weight ratio of balls-to-powder was 30:1. Milling resulted in a significant reduction of the grain size. The grain sizes of the  $\text{TiO}_2$  and  $\text{Al}_2\text{O}_3$  were calculated from the full width at half-maximum (FWHM) of the diffraction peak

\*Corresponding author:  
Tel : +82-63-270-2381  
Fax: +82-63-270-2386  
E-mail: ijshon@chonbuk.ac.kr

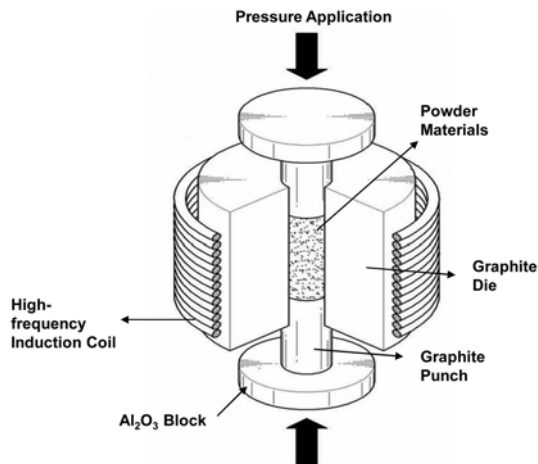


Fig. 1. Schematic diagram of the apparatus for high-frequency induction heated sintering.

by Suryanarayana and Grant Norton's formula [14]:

$$B_r (B_{\text{crystalline}} + B_{\text{strain}}) \cos\theta = k\lambda / L + \eta \sin\theta \quad (1)$$

where  $B_r$  is the full width at half-maximum (FWHM) of the diffraction peak after instrumental correction;  $B_{\text{crystalline}}$  and  $B_{\text{strain}}$  are the FWHMs caused by a small grain size and internal stress, respectively;  $k$  is a constant (with a value of 0.9);  $\lambda$  is the wavelength of the X-ray radiation;  $L$  and  $\eta$  are the grain size and internal strain, respectively; and  $\theta$  is the Bragg angle. The parameters  $B$  and  $B_r$  follow Cauchy's form with the relationship:  $B = B_r + B_s$ , where  $B$  and  $B_s$  are the FWHMs of the broadened Bragg peaks and the standard sample's Bragg peaks, respectively.

The powders were placed in a graphite die (outside diameter, 45 mm; inside diameter, 20 mm; height, 40 mm) and then introduced into the high-frequency induction heating sintering (HFIHS) apparatus shown schematically in Fig. 1. The HFIHS apparatus includes a 15 kW power supply which provides an induced current through the sample, and a 50 kN uniaxial press. The system was first evacuated and a uniaxial pressure of 80 MPa was applied. An induced current was then activated and maintained until the densification rate was negligible, as indicated by the real-time output of the shrinkage of the sample. The shrinkage was measured by a linear gauge measuring the vertical displacement. The HFIHS can be controlled in two ways: by temperature control or by output control. The latter was chosen to investigate the effect of the output of the total power, given that the induced current level has a direct effect on the rate of heating and on the maximum temperature. The output level was 80% output of the total power. Temperatures were measured by a pyrometer focused on the surface of the graphite die. At the end of the process, the induced current was turned off and the sample cooled to room temperature. The process was carried out under a vacuum of 5.33 Pa.

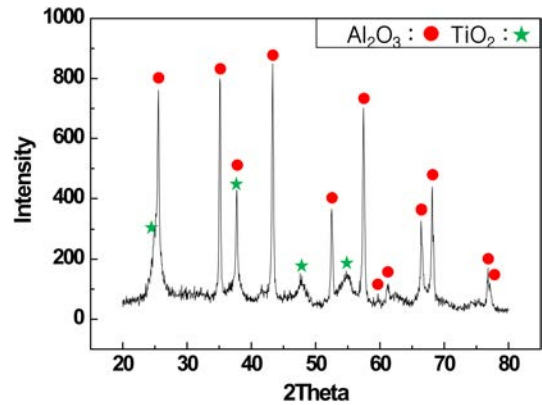


Fig. 2. X-ray diffraction patterns of the  $\text{Al}_2\text{O}_3$  and  $\text{TiO}_2$  powders milled for 4 h.

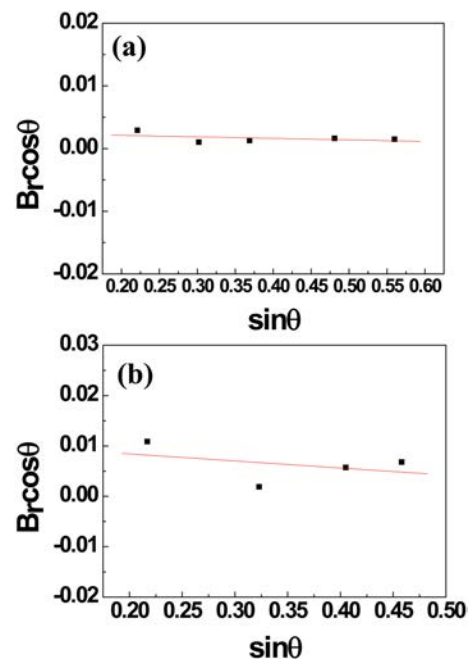


Fig. 3. Plot of  $B_r (B_{\text{crystalline}} + B_{\text{strain}}) \cos\theta$  versus  $\sin\theta$  for  $\text{Al}_2\text{O}_3$  (a) and  $\text{TiO}_2$  (b) powder milled for 4 h.

The relative density of the sintered sample was measured by the Archimedes method. Microstructural information was obtained from product samples, which had been polished and etched using thermal etching for 1 h at 1100 °C. Compositional and microstructural analyses of the products were made through X-ray diffraction (XRD), field emission scanning electron microscope (FE-SEM) with energy dispersive X-ray spectroscopy (EDS). Vickers hardness was measured by performing indentations at a load of 5 kg and a dwell time of 15 s.

## Results and discussion

Fig. 2 shows X-ray diffraction patterns of the  $\text{TiO}_2$ - $\text{Al}_2\text{O}_3$  powders after high-energy ball milling for 4 h.  $\text{TiO}_2$  and  $\text{Al}_2\text{O}_3$  peaks only are detected. Fig. 3 shows a plot of  $B_r \cos\theta$  versus  $\sin\theta$  of  $\text{TiO}_2$  and  $\text{Al}_2\text{O}_3$  milled for 4 h to calculate the particle sizes from XRD data. The

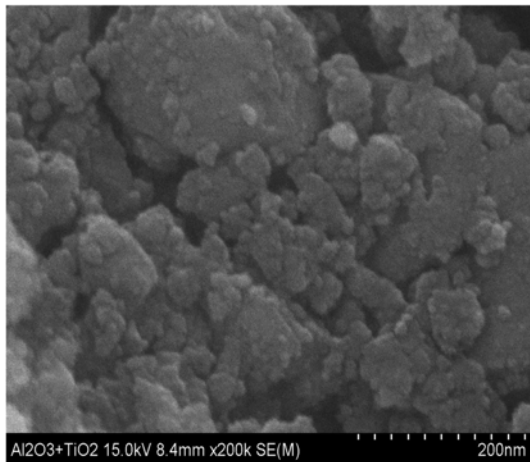


Fig. 4. FE-SEM image of the  $Al_2O_3$  and  $TiO_2$  powders milled for 4 h.

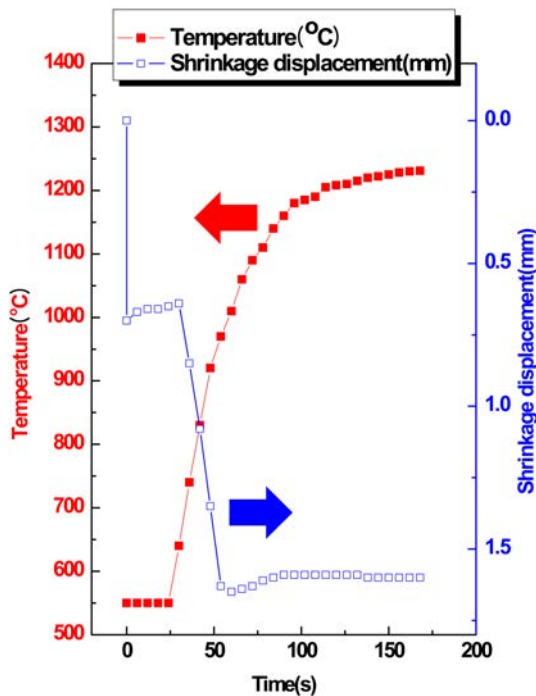


Fig. 5. Variations of temperature and shrinkage with heating time during the sintering of  $Al_2O_3$  and  $TiO_2$  powders milled for 4 h.

average grain sizes of the milled  $TiO_2$  and  $Al_2O_3$  powders determined by Suryanarayana and Grant Norton's formula were about 12 and 53 nm, respectively.

FE-SEM image of the  $TiO_2$  and  $Al_2O_3$  powders milled for 4 h is shown in Fig. 4.  $TiO_2$  and  $Al_2O_3$  powders have a round shape, refinement with milling and some agglomeration. The variations of the shrinkage displacement and temperature with the heating time for 80% of the total output power capacity (15 kW) during the sintering of the high energy ball milled  $TiO_2$  and  $Al_2O_3$  powders under a pressure of 80 MPa are shown in Fig. 5. The application of the induced current resulted in shrinkage due to consolidation. As the induced current was applied, thermal expansion occurred. And then the

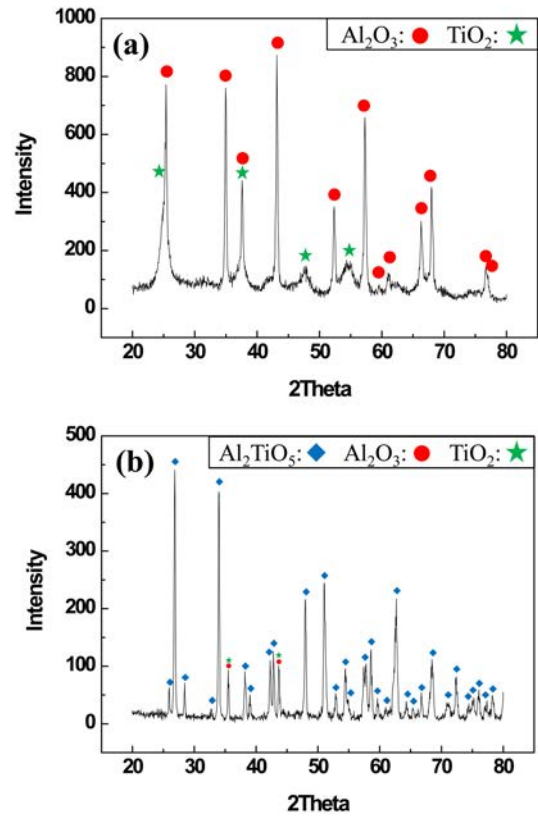


Fig. 6. XRD patterns of specimens sintered at 650 °C (a) and 1250 °C (b) from the high energy ball milled  $TiO_2$  and  $Al_2O_3$  powders.

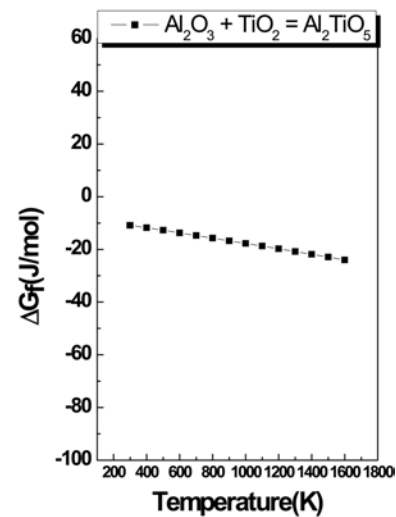


Fig. 7. Temperature dependence of the Gibbs free energy for the formation of  $Al_2TiO_5$ .

shrinkage abruptly increased at about 700 °C. Fig. 6 shows the XRD patterns of specimens sintered at 650 °C (a) and 1250 °C (b) from the high energy ball milled  $TiO_2$  and  $Al_2O_3$  powders. In Fig. 6(a),  $TiO_2$  and  $Al_2O_3$  peaks are detected. But in Fig. 6(b),  $Al_2TiO_5$  peaks are mainly detected. The interaction between these phases, i.e.,



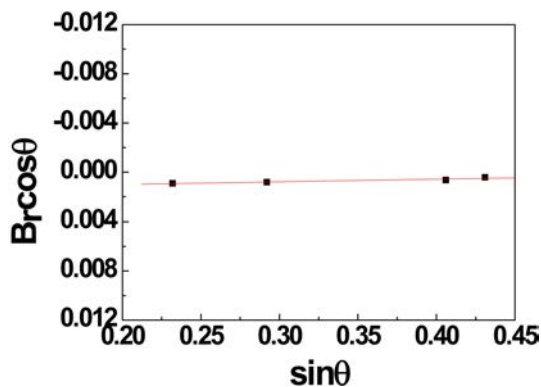


Fig. 8. Plot of  $B_r$  ( $B_{\text{crystalline}} + B_{\text{strain}}$ )  $\cos\theta$  versus  $\sin\theta$  for  $\text{Al}_2\text{TiO}_5$  sintered from the  $\text{Al}_2\text{O}_3$  and  $\text{TiO}_2$  powders milled for 4 h.



Fig. 9. FE-SEM image of sintered  $\text{Al}_2\text{TiO}_5$ .

is thermodynamically feasible as shown in Fig. 7 [15].

A plot of  $B_r$  ( $B_{\text{crystalline}} + B_{\text{strain}}$ )  $\cos\theta$  versus  $\sin\theta$  of  $\text{Al}_2\text{TiO}_5$  in Suryanarayana and Grant Norton's formula [14] is shown in Fig. 8. The average grain size of the  $\text{Al}_2\text{TiO}_5$  systems calculated from the XRD data using Suryanarayana and Grant Norton's formula was about 95 nm. Thus, the average grain size of the sintered  $\text{Al}_2\text{TiO}_5$  is not greatly larger than that of the initial powder, indicating the absence of much grain growth during sintering. This retention of the grain size is attributed to the high heating rate and the relatively short term exposure of the powders to the high temperature. A FE-SEM image of  $\text{Al}_2\text{TiO}_5$  sintered from  $\text{TiO}_2$  and  $\text{Al}_2\text{O}_3$  powders milled for 4 h is shown in Fig. 9.  $\text{Al}_2\text{TiO}_5$  consists of nanocrystallines.

The role of the current (resistive or inductive) in sintering and or synthesis has been the focus of several attempts aimed at providing an explanation to the observed enhancement of sintering and the improved characteristics of the products. The role played by the current has been variously interpreted, the effect being explained in terms of fast heating rate due to Joule heating, the presence of a plasma in the pores separating powder particles, and the intrinsic contribution of the current to mass transport [16-19].

Vickers hardness measurements were performed on polished sections of the  $\text{Al}_2\text{TiO}_5$  samples using a 5 kg load and 15 s dwell time. The Vickers hardness of  $\text{Al}_2\text{TiO}_5$  sintered from  $\text{Al}_2\text{O}_3$  and  $\text{TiO}_2$  powders milled for 4 h was 575  $\text{kg}/\text{mm}^2$ .

Indentations with large enough loads produced median cracks around the indent. The length of these cracks permits the estimation of the fracture toughness of the materials by means of the expression [20]:

$$K_{IC} = 0.204(c/a)^{-3/2} \cdot H_v \cdot a^{1/2} \quad (3)$$

where  $c$  is the trace length of the crack measured from the center of the indentation,  $a$  is one half of the average length of the two indent diagonals, and  $H_v$  is the hardness. The calculated fracture toughness value for the  $\text{Al}_2\text{TiO}_5$  compound sintered from  $\text{Al}_2\text{O}_3$ - $\text{TiO}_2$  powders is about 2.5  $\text{MPa} \cdot \text{m}^{1/2}$ . As in the case of the hardness value, the toughness value is the average of five measurements. The absence of reported values for hardness and toughness on  $\text{Al}_2\text{TiO}_5$  precludes making direct comparison to the results obtained in this study to show the influence of grain size.

## Summary

Nanopowders of  $\text{Al}_2\text{O}_3$  and  $\text{TiO}_2$  were made by high energy ball milling. Using the new rapid sintering method, HFIHS, the densification of nanostructured  $\text{Al}_2\text{TiO}_5$  compound was accomplished within 3 minutes from mechanically activated powders using high energy ball milling. The average grain size of the  $\text{Al}_2\text{TiO}_5$  compound was about 95 nm. The Vickers hardness and fracture toughness of  $\text{Al}_2\text{TiO}_5$  compound sintered from  $\text{Al}_2\text{O}_3$  and  $\text{TiO}_2$  powders milled for 4 h were 575  $\text{kg}/\text{mm}^2$  and 2.5  $\text{MPa} \cdot \text{m}^{1/2}$ , respectively.

## Acknowledgement

This work is partially supported by KIST Future Resource Research Program and by the Human Resources Development of the Korea Institute of Energy Technology Evaluation and Planning (KETEP) grant funded by the Korea government Ministry of Knowledge Economy (No. 20114030200060).

## References

1. M. Ishitsuka, T. Sato, T. Endo, M. Shimada, J. Am. Ceram. Soc. 70 (1987) 69-75.
2. M. Takahashi, M. Fukuda, H. Fukuda, T. Yoko, J. Am. Ceram. Soc. 85 (2002) 3025-3030.
3. M. Sherif El-Eskandarany, J. Alloys & Compounds 305 (2000) 225-238.
4. Fu L, Cao LH, Fan YS, Scripta Materialia 44 (2001) 1061-1068.
5. Niihara K, Niihara A, Advanced structural Inorganic Composite, Elsevier Scientific Publishing Co., Trieste,

- Italy (1990).
6. Berger S, Porat R, Rosen R, Progress in Materials 42 (1997) 311-320.
  7. Fang Z, Eason JW, Int. J. of Refractory Met. & Hard Mater 13 (1995) 297-303.
  8. A.I.Y. Tok, L.H. Luo, F.Y.C. Boey, Materials Science and Engineering A 383 (2004) 229-234.
  9. In-Jin Shon, Hee-Ji Wang, Chang-Yul Suh, Sung-Wook Cho, Wonbaek Kim, Kor. J. Met. Mater. 49 (2011) 347-379.
  10. J. Jung, S. Kang, Scripta Materialia 56 (2007) 561-564.
  11. S.L. Du, S.H. Cho, I.Y. Ko, J.M. Doh, J.K. Yoon, S.Y. Park, I.J. Shon, Kor. J. Met. Mater. 49 (2011) 231-236.
  12. H.S. Kang, I.Y. Ko, J.K. Yoon, J.M. Doh, K.T. Hong, I.J. Shon, Met. Mater. Inter. 17 (2011) 57-61.
  13. N.R. Park, I.Y. Ko, J.M. Doh, J.K. Yoon, I.J. Shon, Journal of Ceramic Processing Research 12 (2011) 660-663.
  14. C. Suryanarayana, M. Grant Norton, X-ray Diffraction A Practical Approach, Plenum Press, New York (1998).
  15. O. Knacke, O. Kubaschewski, K. Hesselmann, Thermochemical Properties of Inorganic Substances, Springer-Verlag (1991).
  16. Z. Shen, M. Johnsson, Z. Zhao and M. Nygren, J. Am. Ceram. Soc. 85 (2002) 1921-1927.
  17. J.E. Garay, U. Anselmi-Tamburini, Z.A. Munir, S.C. Glade and P. Asoka- Kumar, Appl. Phys. Lett. 85 (2004) 573-575.
  18. J.R. Friedman, J.E. Garay. U. Anselmi-Tamburini and Z.A. Munir, Intermetallics. 12 (2004) 589-597.
  19. J.E. Garay, J.E. Garay. U. Anselmi-Tamburini and Z.A. Munir, Acta Mater., 51 (2003) 4487-4495.
  20. K. Niihara, R. Morena, and D. P. H. Hasselman, J.Mater. Sci. Lett. 1 (1982) 12-16.